



Single Cell Analysis of Blood Mononuclear Cells Stimulated Through Either LPS or Anti-CD3 and Anti-CD28

Nathan Lawlor¹, Djamel Nehar-Belaid¹, Jessica D.S. Grassmann¹, Marlon Stoeckius², Peter Smibert², Michael L. Stitzel^{1,3,4}, Virginia Pascual⁵, Jacques Banchereau^{1*†}, Adam Williams^{1,3,4*†} and Duygu Ucar^{1,3,4*†}

¹ The Jackson Laboratory for Genomic Medicine, Farmington, CT, United States, ² New York Genome Center, New York, NY, United States, ³ Institute of Systems Genomics, University of Connecticut, Farmington, CT, United States, ⁴ Department of Genetics and Genome Sciences, University of Connecticut, Farmington, CT, United States, ⁵ Ronay Menschel Professor of Pediatrics, Drukier Institute, Weill Cornell Medicine, New York, NY, United States

OPEN ACCESS

Edited by:

Manuela Mengozzi,
Brighton and Sussex Medical School,
United Kingdom

Reviewed by:

Matthew Collin,
Newcastle University, United Kingdom
Sagar,
University Hospital Freiburg, Germany

*Correspondence:

Jacques Banchereau
jacques.banchereau@jax.org
Adam Williams
adam.williams@jax.org
Duygu Ucar
duygu.ucar@jax.org

[†]These authors have contributed
equally to this work

Specialty section:

This article was submitted to
Inflammation,
a section of the journal
Frontiers in Immunology

Received: 01 December 2020

Accepted: 22 February 2021

Published: 17 March 2021

Citation:

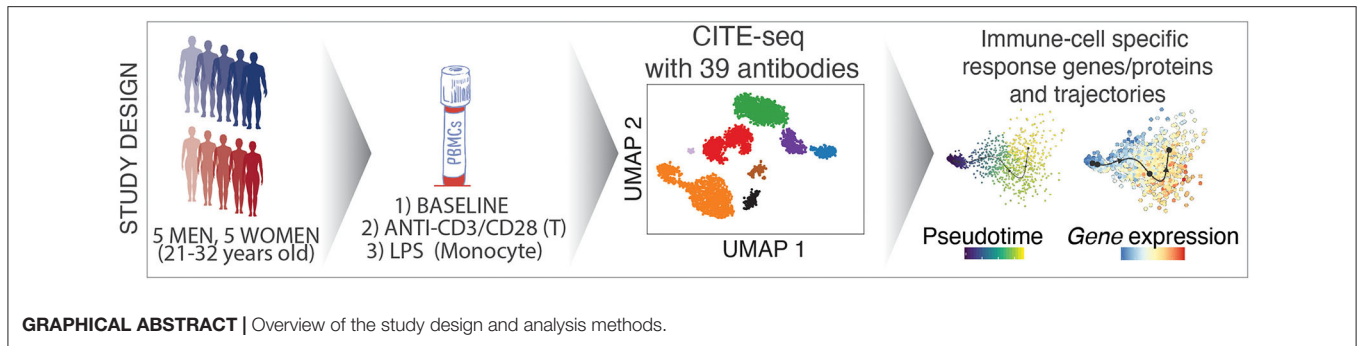
Lawlor N, Nehar-Belaid D, Grassmann JDS, Stoeckius M, Smibert P, Stitzel ML, Pascual V, Banchereau J, Williams A and Ucar D (2021) Single Cell Analysis of Blood Mononuclear Cells Stimulated Through Either LPS or Anti-CD3 and Anti-CD28. *Front. Immunol.* 12:636720. doi: 10.3389/fimmu.2021.636720

Immune cell activation assays have been widely used for immune monitoring and for understanding disease mechanisms. However, these assays are typically limited in scope. A holistic study of circulating immune cell responses to different activators is lacking. Here we developed a cost-effective high-throughput multiplexed single-cell RNA-seq combined with epitope tagging (CITE-seq) to determine how classic activators of T cells (anti-CD3 coupled with anti-CD28) or monocytes (LPS) alter the cell composition and transcriptional profiles of peripheral blood mononuclear cells (PBMCs) from healthy human donors. Anti-CD3/CD28 treatment activated all classes of lymphocytes either directly (T cells) or indirectly (B and NK cells) but reduced monocyte numbers. Activated T and NK cells expressed senescence and effector molecules, whereas activated B cells transcriptionally resembled autoimmune disease- or age-associated B cells (e.g., CD11c, T-bet). In contrast, LPS specifically targeted monocytes and induced two main states: early activation characterized by the expression of chemoattractants and a later pro-inflammatory state characterized by expression of effector molecules. These data provide a foundation for future immune activation studies with single cell technologies (<https://czi-pbmc-cite-seq.jax.org/>).

Keywords: immune responses, single cell profiling, immune cell activation, LPS, antiCD3/CD28, CITE-seq, peripheral blood mononuclear cells

INTRODUCTION

The immune system plays a central role not only in fighting infections, but also in the pathogenesis of many diseases. While access to disease-relevant tissues may be limited, blood profiling provides a minimally invasive method to assess immune function and health (1, 2). Blood serves as a conduit for transport of immune cells throughout the body and circulating immune cells frequently display signatures of disease or immune dysfunction (i.e., immunosenescence) (3–5). Transcriptional profiling of blood provides an unbiased method for immune monitoring and has proved invaluable in uncovering novel disease mechanisms. *In vitro* activation of immune cells



is an effective way to assess their functional capacity. For example, T cells can be activated with non-specific mitogens such as PHA (phytohemagglutinin) and ConA (Concanavalin A) (6), or more specifically through the T cell receptor and co-stimulatory receptors, either by crosslinking with antibodies against CD3 and CD28 (7), or with antigen-laden antigen presenting cells (8). Similarly, innate cells, including monocytes, can be activated through pattern recognition receptors (PRRs) with pathogen-associated molecular patterns (PAMPs) such as lipopolysaccharide (LPS) (9). Studying such cellular responses is an effective strategy to uncover functional defects and/or disease-associated phenotypes in human immune cells, and has been widely applied to autoimmune diseases (10–12), immunodeficiency, aging (13–16), and allergy (17).

Advances in single cell technologies can precisely uncover donor-, cell type-, and cell state-specific variation in immune cell functions from clinical samples containing mixed cell populations (18, 19). Hence, these technologies are increasingly used to study *ex vivo* and *in vitro* cellular responses of diverse immune cell types [CD8⁺ T cells (20, 21), dendritic cells (DCs) (22, 23), and B cells (24)] as well as activated cells in immune diseases (25). However, single cell gene expression profiling of activated cells has unique data generation and analysis challenges including identifying and removing multiplet cells that increase in number as cellular interactions increase upon activation. Furthermore, avoiding batch effects is essential to distinguish activation-specific gene expression patterns from batch-induced changes. Another major limitation is the high cost of the methodology which prevents large scale studies. Recent advances can address some of these challenges. For example, multiplexing *via* hashtag oligonucleotides (26) and individuals' genotypes (27) permits simultaneous sequencing of libraries from multiple individuals and conditions to reduce both the cost and technical batch effects. Finally, cellular indexing of transcriptomes and epitopes by sequencing (CITE-seq) technology (26) profiles epitopes (i.e., cell surface proteins) and gene expression levels from the same single cells and is particularly suitable for studying distinct immune cell types and states (e.g., activated and resting) and for filtering out multiplets among activated cells.

We combined cell hashing and genotype-based multiplexing to generate CITE-seq data for the deep analysis of circulating human immune cell responses to classic activators of adaptive (anti-CD3/CD28) and innate (LPS) immune cells. Responses to

these activators have been studied over decades (6) *via* bulk profiling of sorted cells in a reductionist manner, which missed indirect effects of these activators on other cell types as well as the heterogeneity in responses at the single cell level. PBMCs from 10 healthy young donors were profiled at baseline and following activation *via* (1) anti-CD3 + anti-CD28 for selective T cell activation, or (2) LPS for monocyte activation using CITE-seq to quantify changes in both transcript and protein levels using 39 antibodies (e.g., CD3, CD4, CD14, CD56, CD69, CD25). Data from this study uncovered cell-specific responses to each condition at both the gene and protein level and uncovered direct and indirect effects of these activators on immune cell transcriptomes. This study will guide future single cell studies of activated immune cells in health and disease (<https://czi-pbmc-cite-seq.jax.org/>).

RESULTS

Simultaneous Protein and Gene Expression Profiling of Resting and Activated PBMCs

PBMCs were isolated from the blood of 10 healthy young individuals (5 men, 5 women; 21–32 years old; Caucasian), and were cultured for 24 h with LPS (10 ng/ml), anti-CD3/CD28 (2 μg/ml each) (section Methods), or in medium alone (referred to as “Baseline”). Flow cytometry analysis confirmed that anti-CD3/CD28 treatment induced the expression of activation markers (CD25, CD69) on T cells (Figures 1A,B), whereas LPS activated monocytes as shown by CD80 induction (Figures 1C,D). To study the effects of these activation conditions at the single cell level, we pooled baseline and activated cells from the 10 individuals (30 samples in total) and used CITE-seq to simultaneously profile changes in levels of transcripts and 39 cell surface proteins (Supplementary Table 1). To reduce experimental batch effects and costs, equal numbers of cells from all donors and conditions were pooled and sequenced together. Cells from different conditions were labeled with Cell Hashing Antibodies (BioLegend) (Figure 1E), where three hashtag oligonucleotides (HTOs) were used to demultiplex data from each experimental condition (baseline, LPS, anti-CD3/CD28) using a Gaussian mixture model on HTO counts (Supplementary Figure 1A). Finally, donor genotypes were used to demultiplex data from each individual with *Demuxlet* (27) (Figure 1F).

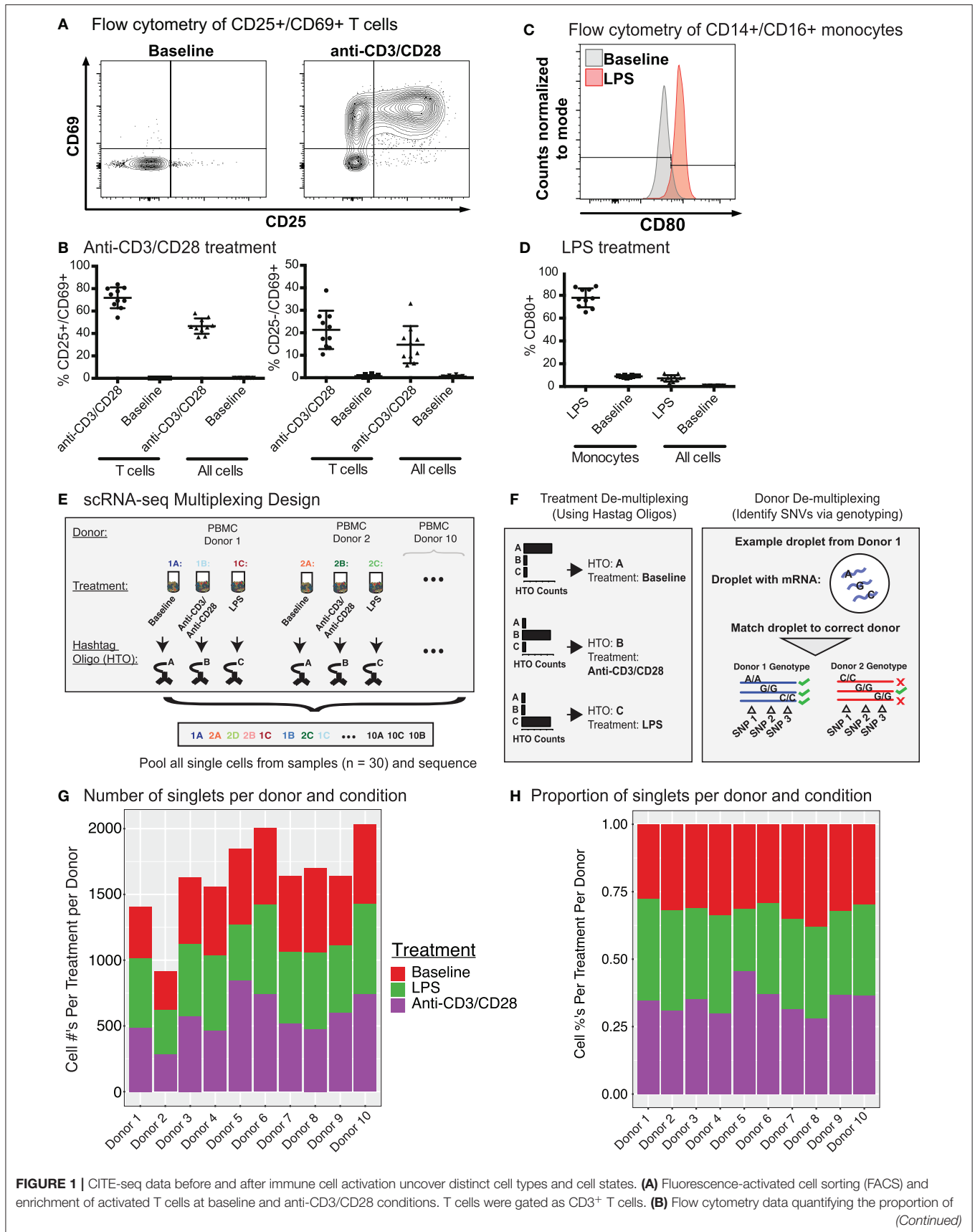


FIGURE 1 | activated cells (CD25⁺ CD69⁺ or CD25⁻ CD69⁺) after anti-CD3/CD28 stimulation. All cells = number of activated T cells as a percentage of all PBMCs; T cells = numbers of activated T cells as a percentage of all CD3⁺ T cells. **(C)** Distributions of CD80 expression in sorted monocytes and all PBMCs at baseline and LPS conditions. **(D)** Flow cytometry proportions of activated monocytes (CD80⁺) before and after LPS stimulation. All cells = number of activated monocytes as a percentage of all PBMCs; Monocytes = number of activated monocytes as a percentage of CD14⁺CD16⁺ monocytes. **(E)** Sample multiplexing was performed using cell hashtag oligonucleotide (HTO) antibodies, where a different HTO barcode was used for a specific treatment condition (e.g., HTO A for cells under baseline condition). **(F)** De-multiplexing of treatment information using HTOs (left), and donor of origin information using genetic variation across donors in the form of single nucleotide variations (SNVs)(right). **(G)** Numbers and **(H)** proportions of singlet cells retained per donor per condition after removing multiplet cells.

Overall, 195,480 droplets were captured from all samples (**Supplementary Table 2**).

Cell multiplets from different sources were detected and eliminated with the help of multiplexing strategies (HTOs and genotypes) and the levels of cell-specific marker proteins (**Supplementary Figure 1B**, section Methods). HTOs uncovered multiplets from different treatment conditions, which constituted ~13% (26,084/195,480) of total droplets in addition to 18,871 (~9%) empty droplets (i.e., no HTO detected) (**Supplementary Figure 1C**). Using genotypes, we identified and filtered out multiplets from different individuals as well as cells that could not be assigned to an individual with high confidence (i.e., ambiguous) (**Supplementary Figure 1D**), resulting in 55,353 single cells with a mean of 1,932 unique molecular identifiers (UMIs) per cell. Empty droplets from cell hashing and ambiguous cells from *Demuxlet* overlapped extensively (83%, **Supplementary Figure 1E**). Finally, expression levels of cell type-specific proteins uncovered multiplets from different cell types (section Methods). After multiplet removal and demultiplexing, an average of 1,638 (range 914–2,034) cells per donor were detected (16,382 total cells) (**Figure 1G**), with 855 genes detected per cell on average. Donors showed similar cell frequency distributions across conditions (**Figure 1H**). The proportions of CD25⁺/CD69⁺ T cells from CITE-seq and flow cytometry data were highly correlated (Pearson's $R = 0.96$) (**Supplementary Figure 1F**) across individuals upon anti-CD3/CD28 stimulation, indicating that CITE-seq is an effective technology to capture and study immune cell activation.

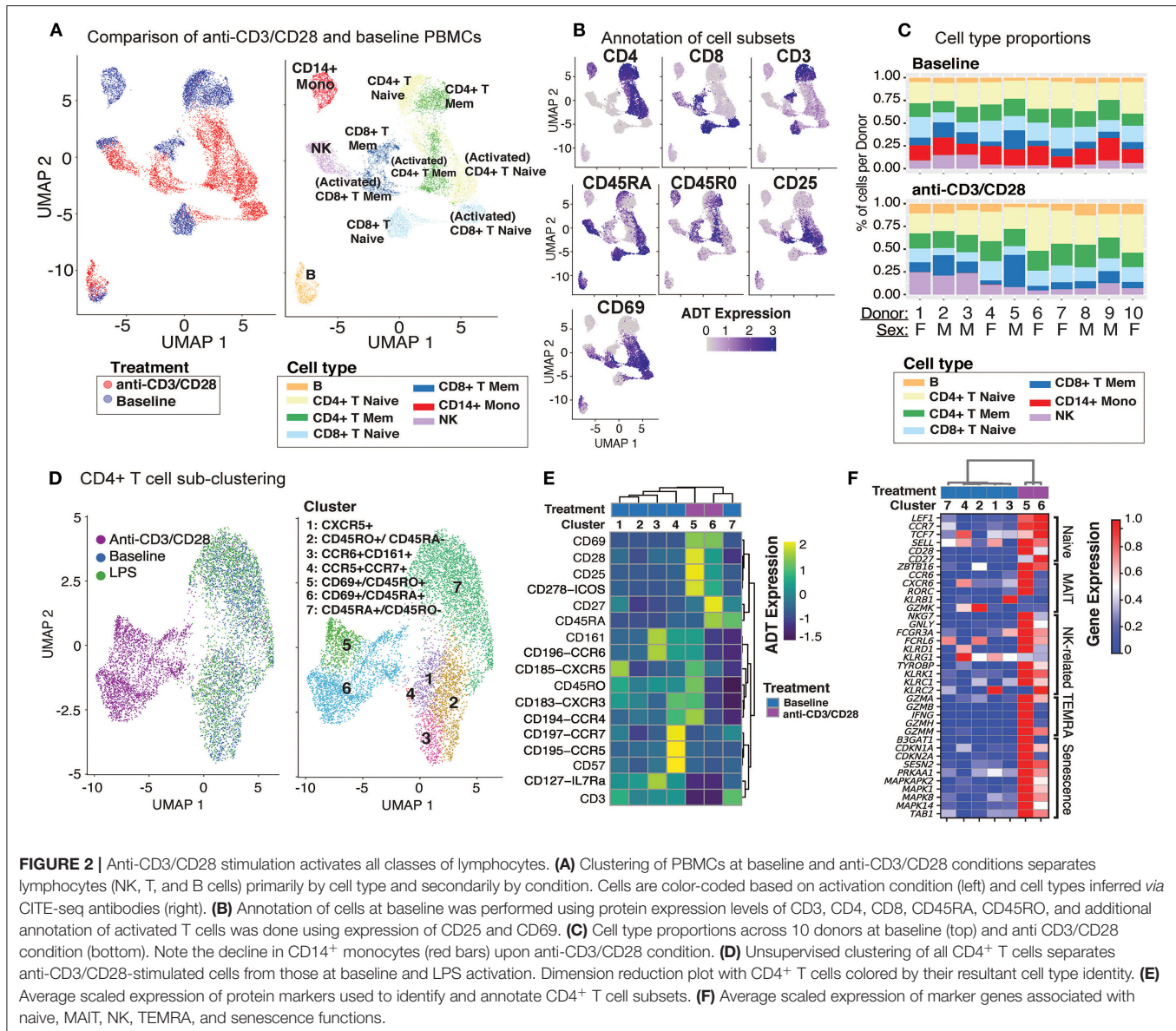
Anti-CD3/CD28 Treatment Activates All Classes of Lymphocytes

Baseline and anti-CD3/CD28-activated PBMCs were jointly analyzed using the top 500 most variably expressed genes and proteins (**Figure 2A**; section Methods). Cell clusters were annotated using the expression of marker proteins: CD19 and CD20 for B cells, CD16 and CD56 for NK cells, CD14 and CD11c for CD14⁺ monocytes, CD3 and CD4 for CD4⁺ T cells, CD3 and CD8a for CD8⁺ T cells, and CD45RA and CD45RO for naïve and memory T cells, respectively (**Figure 2B** and **Supplementary Figure 2A**). Accordingly, baseline PBMCs from 10 individuals consisted of 60–82% T cells, 12–25% CD14⁺ monocytes, 4–15% NK cells, and 3–6% B cells (**Figure 2C**), which was highly correlated with flow cytometry data from this cohort (**Supplementary Figure 2B**; Pearson's $R = 0.97$). CD8⁺ memory T cells were the most variable cell type between individuals with a coefficient of variation (CV) of 0.65, followed by NK cells (CV = 0.51).

Anti-CD3/CD28 treatment activated all lymphocytes (**Figure 2A**, left). PBMCs grouped primarily by cell type and secondarily by cell state (i.e., resting vs. activated) based on their annotations with cell surface markers (**Figure 2B** and **Supplementary Figure 2A**). Labeled antibodies allowed the detection of naïve (CD45RA^{high}) and memory (CD45RO^{high}) T cells. Activated T cells showed early (CD69) and late (CD25) activation markers and reduced CD3 expression (**Figure 2B**). Indirect activation of NK and B cells was revealed by the induction of CD69 mRNA and protein (**Figure 2B**). Notably, this treatment caused a significant decline in monocyte numbers and their percentages in PBMCs (**Figure 2C**). This is likely due to the induction of apoptosis in monocytes *via* activated T cells (28, 29) as apoptosis-associated genes were upregulated (e.g., *CTSL*, *TRAF1*, *TNF*, and *GZMB*) among T cell-monocyte multiplets detected in the anti-CD3/CD28 condition.

Senescence and Cytotoxicity Molecules Are Upregulated in Activated CD4⁺ T Cells

Unsupervised clustering of CD4⁺ T cells using both gene and protein expression levels revealed 7 subgroups: 5 found at baseline and 2 additional ones following activation with anti-CD3/CD28 (**Figure 2D**). CD4⁺ cells did not respond to LPS activation and clustered with baseline cells. At baseline, we detected CD45RA⁺CD45RO⁻ (cluster 7; naïve cells) and CD45RA⁻CD45RO⁺ (cluster 2; memory cells) subsets as well as less abundant CD45RO⁺CCR6⁺CD161⁺ (cluster 3; memory cells including Th17 cells), CD45RO⁺CXCR5⁺ (cluster 1; memory cells including Tfh cells), and CD45RO⁺CD57⁺CCR5⁺CCR7⁺ cells (cluster 4; other memory cells). CD45RO⁺CXCR5⁺ cells, which constituted ~8% of baseline CD4⁺ T cells (3–14% between donors) (**Supplementary Figure 2C**) were in an apparent resting state as they lacked ICOS (CD278) and CD69, in alignment with our previous observations (30). Cluster 3 cells (**Figures 2D,E**) expressed chemokine receptor CCR6 (indicating tissue-specific homing properties) and C-type lectin receptor CD161 (*KLRB1*) and CD127 (*IL7R*) on their surface constituted ~9.9% of CD4⁺ T cells (**Supplementary Figure 2C**). Finally, we identified a smaller subset of memory cells that highly expressed CD57, CCR5, and CCR7 on their surface in addition to moderately expressing CXCR3 and CCR4 (**Figure 2E**) and include Th1 (CCR5 and CXCR3) and Th2 (CCR3, CCR4) subsets (31). Activated CD4⁺ T cells clustered into two groups: cluster 5 (memory activated: CD69⁺ CD45RO⁺) and cluster 6 (naïve activated: CD69⁺ CD45RA⁺). Cells in both clusters expressed co-stimulatory proteins (most notably CD28, CD278) and activation marker proteins (CD69, CD25) (**Figure 2D**). However, the expression



of certain markers decreased upon activation (e.g., CD161, CCR6) limiting our ability to discriminate subsets among activated CD4⁺ T cells. T cell senescence genes (e.g., *SEN2*, *PRKAA1*, *MAPK1*, *TAB1*) were induced both in naïve and memory CD4⁺ T cells upon activation (**Figure 2F**). Moreover, activated memory cells (CD45RO⁺CD45RA⁻CD69⁺) highly expressed genes associated with terminally differentiated effector cells [T cells re-expressing CD45RA (TEMRA)] (32), including cytotoxic molecules (e.g., *GZMA*, *GZMB*, *IFNG*, *GZMH*, *GNLY*) (**Figure 2F** and **Supplementary Table 3**).

Naive T Cell Responses to Anti-CD3/CD28 Stimulation Are Stronger Than Those of Their Memory Counterparts

CD8⁺ T cells were composed of 6 distinct clusters: 4 found at baseline and 2 additional ones upon anti-CD3/CD28

activation. LPS did not activate CD8⁺ T cells as cells treated with LPS clustered together with baseline cells (**Figure 3A**). Baseline clusters included: CD45RA⁺CD45RO⁻ (cluster 4; naïve), CD45RO⁺CD45RA⁻ (cluster 1; memory) cells, CD57⁺CXCR5⁺CD45RO^{high} cells (cluster 2; effector memory cells, ~8.6% of CD8⁺ T cells) and CD161⁺CCR6⁺ cells (cluster 5; MAIT, mucosal-associated invariant T cells, ~7.9% of CD8⁺ T cells) (**Figure 3B** and **Supplementary Figure 2C**). Anti-CD3/CD28 activation elicited a strong response in CD8⁺ T cell subsets (**Figure 3A**), resulting in activated memory cells (cluster 3; CD69⁺CD45RO⁺) and activated naïve cells (cluster 6; CD69⁺CD45RA⁺). Both activated clusters expressed high levels of activation proteins (CD25, ICOS, CD69) (**Figure 3B**). When compared to activated memory cells, activated naïve cells expressed higher levels of the CD27 and CD28 proteins (**Figure 3B**). Cluster 5 cells expressed marker genes of MAIT cells [*RORC*, *KLRB1*, and

CCR6 (33)] (**Figure 3C**). Activated cells from clusters 3 and 6 expressed high levels of both cytotoxic (e.g., *GZMA*, *GZMK*) and senescence genes (*SESN2*, *CDKN1A*, *CDKN2A*) (**Figure 3C**).

Differential expression analyses between activated and resting T cells revealed that 950 genes were upregulated in naïve and memory CD4⁺ and CD8⁺ T cells (**Supplementary Figure 2D**), including *IFNG*, Type I interferon-inducible genes (*ISG15*, *ISG20*), and interferon regulatory factors (*IRF1*, *IRF4*) (**Supplementary Table 4**). Stimulation induced more genes in naïve (CD45RA⁺CD45RO⁻) T cells than memory (CD45RO⁺CD45RA⁻) T cells; 824 transcripts were induced specifically in naïve CD4⁺ and CD8⁺ T cells, while 494 were induced in CD8⁺ naïve T cells (**Supplementary Figure 2D**). Naïve cell-specific response genes were enriched for KEGG pathways associated with cell cycle (e.g., *MCM2/3/5/6*, *CDKN2D*, *SMC1A*, *CHEK1*), carbon metabolism (e.g., *ESD*, *CS*, *SDHD*, *GPI*), and basal transcription factors (e.g., *ETF1*, *EIF4E*, *EIF4H*, *EIF4G1*), emphasizing the proliferative and expansive capacity of naïve T cells upon activation (**Supplementary Table 4**). Pseudo-temporal ordering of baseline and activated T cells using the Slingshot algorithm (34) revealed mostly linear trajectories for activation despite the existence of distinct memory (CD45RO⁺CD45RA⁻) subsets at baseline, thereby indicating that these different subsets respond similarly to anti-CD3/CD28 activation. Distinct subsets (e.g., CD161⁺CCR6⁺) were no longer detectable upon activation—potentially due to internalization of cell surface proteins—preventing further interrogation of their specific responses. Instead, our analyses revealed that, for both CD4⁺ T and CD8⁺ T compartments, activated naïve (CD45RA⁺CD45RO⁻CD69⁺) cells were ordered toward the end of the activation pseudotime trajectories, due to the greater transcriptomic changes in naïve T cells upon anti-CD3/CD28 stimulation compared to memory cells (**Figures 3D,E**). Taken together these data show that anti-CD3/CD28 activation has a significant effect on T cell transcriptomes, where naïve T cells go through more significant changes compared to their memory counterparts.

Anti-CD3/CD28 Activation of PBMCs Result in Indirect Activation of NK Cells

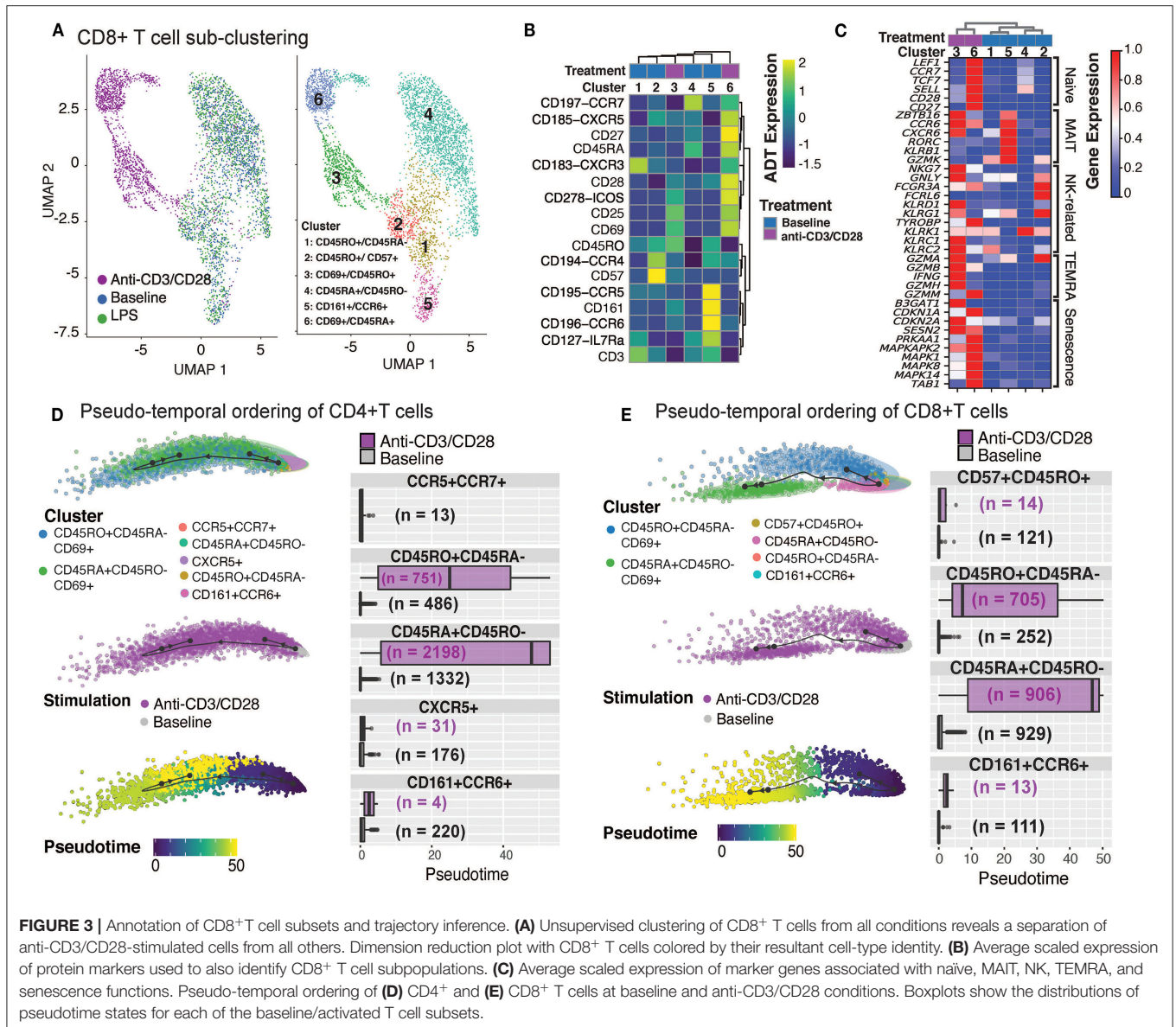
Anti-CD3/CD28 treatment induced CD69 protein expression on NK cells, and transcription of 74 genes (**Supplementary Table 5**), 60 of which were shared with T cells, including cytotoxic molecules (e.g., *GZMB*) as well as interferon response genes (**Supplementary Figure 2D**, **Supplementary Table 4**). Clustering analyses of NK and T cells, at baseline and after anti-CD3/CD28 activation, uncovered the transcriptional similarity between NK and CD8⁺ T cells (**Figure 4A**). Interestingly, activated CD8⁺ T cells clustered distinctly from NK cells likely due to the upregulation of distinct molecules in T cells (**Supplementary Figure 2D**). To further characterize these cells, we derived MAIT, cytotoxicity, and senescence scores using relevant gene sets (section Methods, **Supplementary Table 3**). As expected, CD8⁺CD161⁺CCR6⁺ cells had the highest MAIT score. Activated NK cells (CD56⁺CD69⁺) showed the highest

cytotoxicity score among all studied cell types, followed by activated CD8⁺ memory cells (CD8⁺CD45RO⁺CD69⁺) T cells (**Figure 4B**). In alignment with this, upon activation, important cytotoxic molecules were up-regulated in NK cells, including perforin (*PRF1*), granulysin (*GNLY*), and granzymes (*GZMB*) (**Supplementary Table 5**). In contrast, activated T cells had high senescence scores, particularly for activated naïve CD8⁺ T cells (CD45RA⁺CD69⁺), which was in alignment with the increased expression of *CDKN1A* (encoding p21 protein) and *CDKN2A* (encoding p16 protein) along with other senescence-associated molecules (**Figure 3C**). In contrast, baseline and activated NK cells displayed low senescence scores.

The significant effect of anti-CD3/CD28 treatment on the NK cell transcriptome (**Figure 4C**; left) results from indirect activation, since neither TCR nor CD28 are expressed by NK cells. Unsupervised clustering of NK cells from baseline and anti-CD3/CD28 stimulation identified seven groups (**Figure 4C**; middle), four of which were enriched in activated cells (~95% activated, Clusters 0, 1, 4, and 5) (**Figure 4C**; right). Cells in these four clusters of activated NK cells had higher expression of interferon-stimulated genes (ISGs) including *LY6E*, *IFI6*, and *IFI27* (**Figure 4D**) than NK cells at baseline. One of these clusters (cluster 4) highly expressed marker proteins for activation: *CD69* and *CD83* (35) (**Figure 4D**). NK cells in cluster 4 expressed *XCL1* that facilitates their communication with DCs, as well as *CCL3* and *CCL4* (36) that enable them to recruit various immune cells including naïve CD8⁺ T cells. In contrast, clusters 2, 3, and 6 cells were mostly from the baseline condition and enriched for *KLF2*, which encodes a transcription factor important for NK cell survival (37). Trajectory analyses of NK cells (baseline and activated) revealed that the cells at the end of the trajectory have the highest expression of interferon-gamma (*IFNG*), granzyme B (*GZMB*), *CD69*, and various chemokines (*CCL3*, *CCL4*, *XCL1*, *XCL2*) (**Figure 4E**), resembling the profiles of cluster 4 cells. Expression of other interferon-inducible genes (*IFITM1*, *ISG15*) and granulysin (*GNLY*) peaked prior to the end of the trajectory, highlighting differences in timing and degree of NK subtype activation. Thus, scRNAseq of anti-CD3/CD28 activated PBMCs revealed that NK cells are indirectly activated with this condition that resulted in upregulation of cytotoxic molecules.

Anti-CD3/CD28 Activation of PBMCs Results in B Cell Activation

Upon anti-CD3/CD28 treatment of PBMCs, B cells upregulated 383 genes and 4 cell surface proteins (*CD69*, *CD25*, *ICOS*, *CD38*) (**Figure 5A**, **Supplementary Table 5**). Increased transcription included ribosome and proteasome activity, oxidative phosphorylation machinery, and mitochondrial stress pathways. It also involved genes associated to humoral immune responses and Type 2 interferon signaling, such as *CD40*, *CXCL9*, *CXCL10*, and *IRF1* (**Supplementary Table 5**). Resting and activated B cells clustered into six distinct groups (**Figure 5B**; middle), where clusters 0 (comprising 25% of B cells) and 3 (comprising 15% of B cells) were specifically enriched in activated B cells (>90%) (**Figure 5B**; right). Cells from the activated B cell clusters highly expressed ISGs (*IF44*,

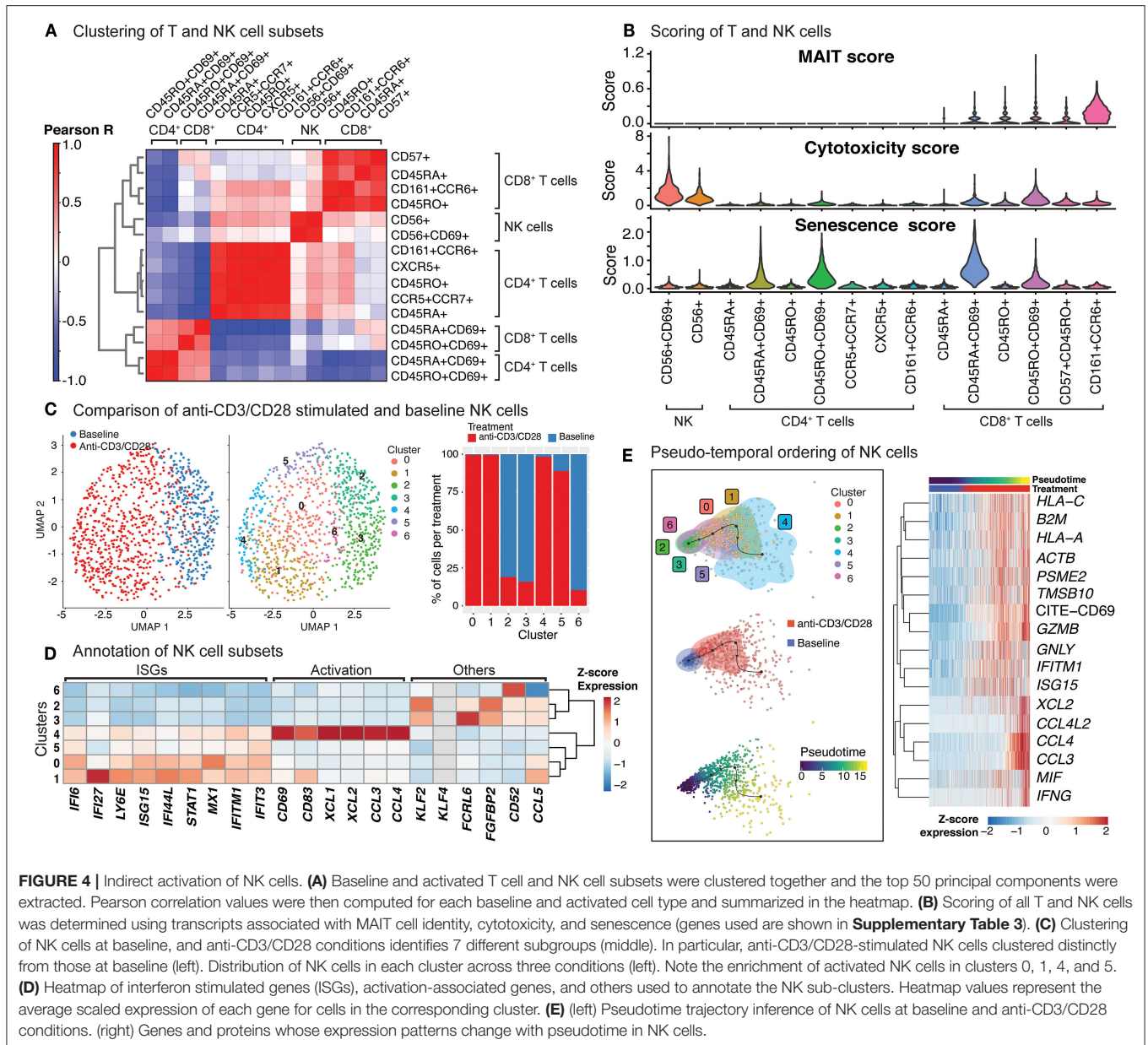


IF44L, *STAT1*, and *MX1*) and the activation marker *CD69* (Figure 5C). Cluster 0 cells expressed genes associated with age-associated B cells (ABC) (38–40) and DN2 cells (41) (e.g., *TLR7*, *PRDM1*, *TGAX/CD11c* and *TBX21/T-bet*). Distinct from ABCs and DN2 cells, they retained follicular (*CXCR5*) and conventional memory (*CD27*) markers. Cluster 3 cells expressed additional markers associated with DN2 cells, such as *FCRL5* and *TRAF5*, but lacked the expression of *TLR7*, *ITGAX*, and *TBX21*. Differences detected between these activated B cells and ABC/DN2 cells may reflect acute vs. chronic activation of B cells as seen with aging and auto-immune diseases. Slingshot analyses revealed mostly linear activation trajectories for B cells, where the cells at the end of the trajectory had the highest expression of activation markers (*CD25*, *CD69*, and *CD278*) as well as genes encoding ribosomal proteins (Figure 5D). Thus, scRNAseq of anti-CD3/CD28 activated PBMCs is providing new

clues to the generation of DN2 cells, that are expanded in SLE (25, 41).

LPS Treatment of PBMCs Only Affects CD14⁺ Monocytes and Induces Inflammation-Associated Genes

Baseline and LPS-activated PBMCs were jointly analyzed using the top 500 most variably expressed genes and proteins (Figure 6A) and were annotated using the expression of marker proteins (section Methods) (Supplementary Figure 3A). LPS stimulation did not lead to significant changes in PBMC cell compositions (Figure 6B). Among PBMCs, only monocytes were activated by the LPS treatment (Figures 6A,C) and showed upregulated expression of pro-inflammatory cytokine genes (e.g., *IL8*, *IL1B*) (Supplementary Figure 3B). To globally assess

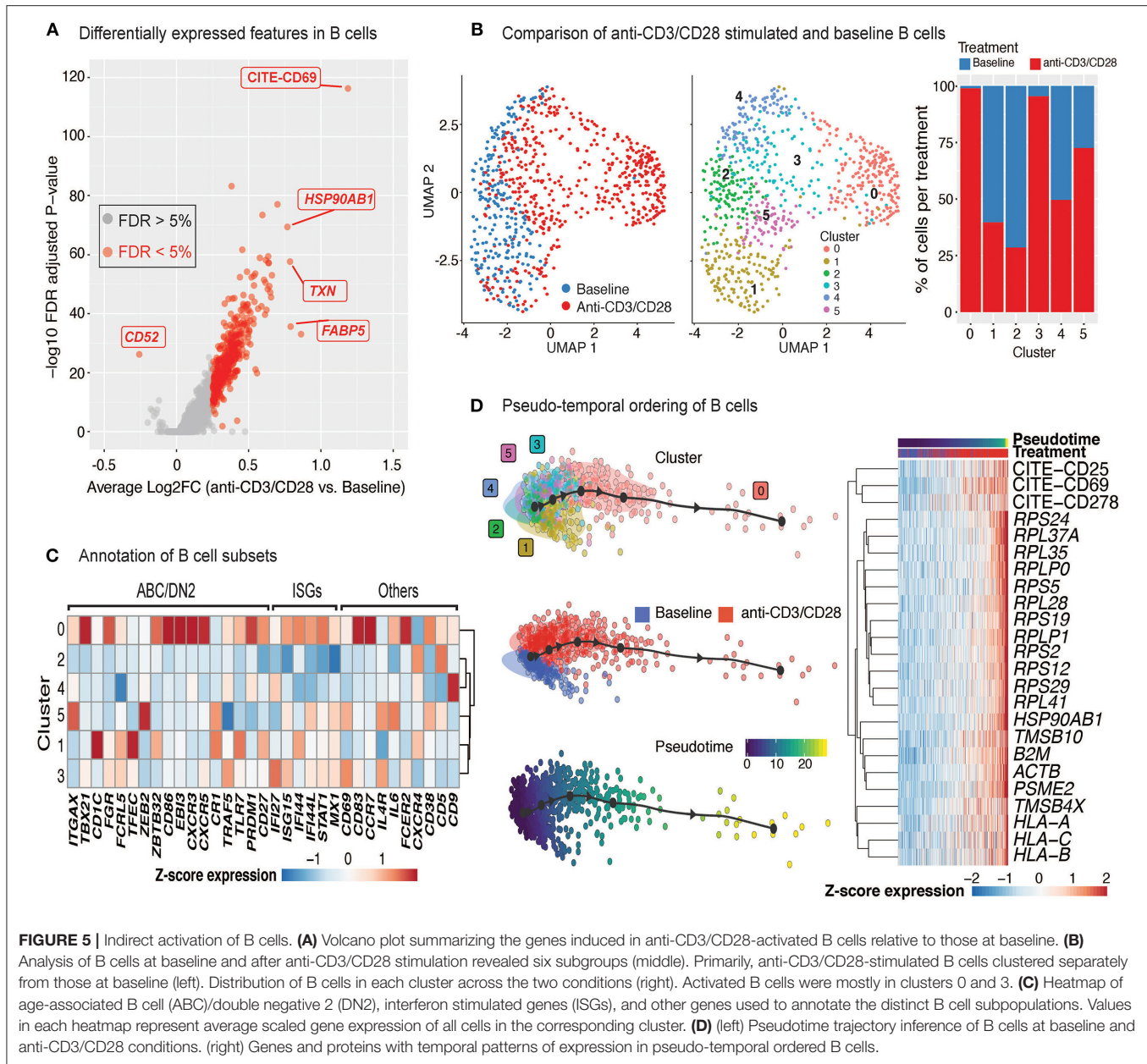


the enrichment of inflammation-associated transcripts in each cell type, we used a reference list of 249 inflammation-related genes from NanoString Technologies Inc. (section Methods). Activated monocytes had significantly higher inflammation scores compared to baseline monocytes and all other cell types (**Figure 6D**). Overall, 219 genes were differentially expressed in monocytes (125 up- and 94 down-regulated; FDR 5%) upon LPS treatment (**Figure 6E** and **Supplementary Table 5**). Functional enrichment analyses of these differentially expressed genes (DEGs) using gene ontology (GO) terms and KEGG pathways (42) revealed that LPS treatment activated pattern recognition receptor signaling pathways (Toll-like and NOD-like) and the pro-inflammatory NF-kappa B signaling pathway (FDR 5%;

Supplementary Table 6, Supplementary Figure 3C), including the up-regulation of important chemokines (*CCL3*, *CCL4*) and cytokines (*IL1B*, *IL6*) (**Figure 6F**). In contrast, LPS stimulation decreased the expression of genes associated with antigen processing and presentation *via* MHC class II and phagosome activity (**Figure 6F, Supplementary Table 6**).

LPS-Activated Monocytes Exhibit Two Distinct Transcriptional States

The Slingshot (34) algorithm revealed that the trajectory of monocytes followed a linear transition from resting to activated states (**Figure 6G**; top, **Supplementary Figure 3D**). LPS-activated monocytes showed increased variation in their transcriptional responses and were positioned at the end of



the trajectory (Figure 6G; top). Genes that are important for defining monocyte trajectories included inflammatory cytokines (*IL6*, *IL8*, *IL1B*), metallothionein genes involved in zinc transport [*MT1F* (43)] and oxidative stress [*MT2A* (44)], as well as alarmins (*S100A8/S100A9*), which induce pro-inflammatory cytokine production (45) (Supplementary Figure 3E). Alarmins and metallothionein gene expression peaked in early stages (pseudotime values 5 up to 15), whereas pro-inflammatory cytokines (e.g., *IL1B*, *IL6*, *IL8*) peaked in late stages (pseudotime ≥ 15) (Figure 6G; bottom, Supplementary Figure 3E). These LPS-induced cellular states and changes were observed consistently across donors (Supplementary Figure 3F). To further dissect this heterogeneity, we clustered baseline

and activated monocytes using k-means clustering ($k = 4$). Baseline monocytes clustered separately from LPS-treated ones (Figure 7A, Supplementary Figure 4A), which were split into 3 clusters referred to as LPS1, LPS2, and LPS3 states. These clusters coincided with the pseudotime values (Supplementary Figure 4B), where LPS1 and LPS2 states mapped to the early activation state and LPS3 mapped to the later inflammatory state (Supplementary Figure 4B). These four monocyte clusters were detected in all individuals (Figure 7B); inflammation scores of clusters (section Methods) increased in agreement with their position in the trajectory, LPS3 having the highest inflammation score (Figure 7C). LPS2 and LPS3 states had the most distinct transcriptional response profiles, with 50

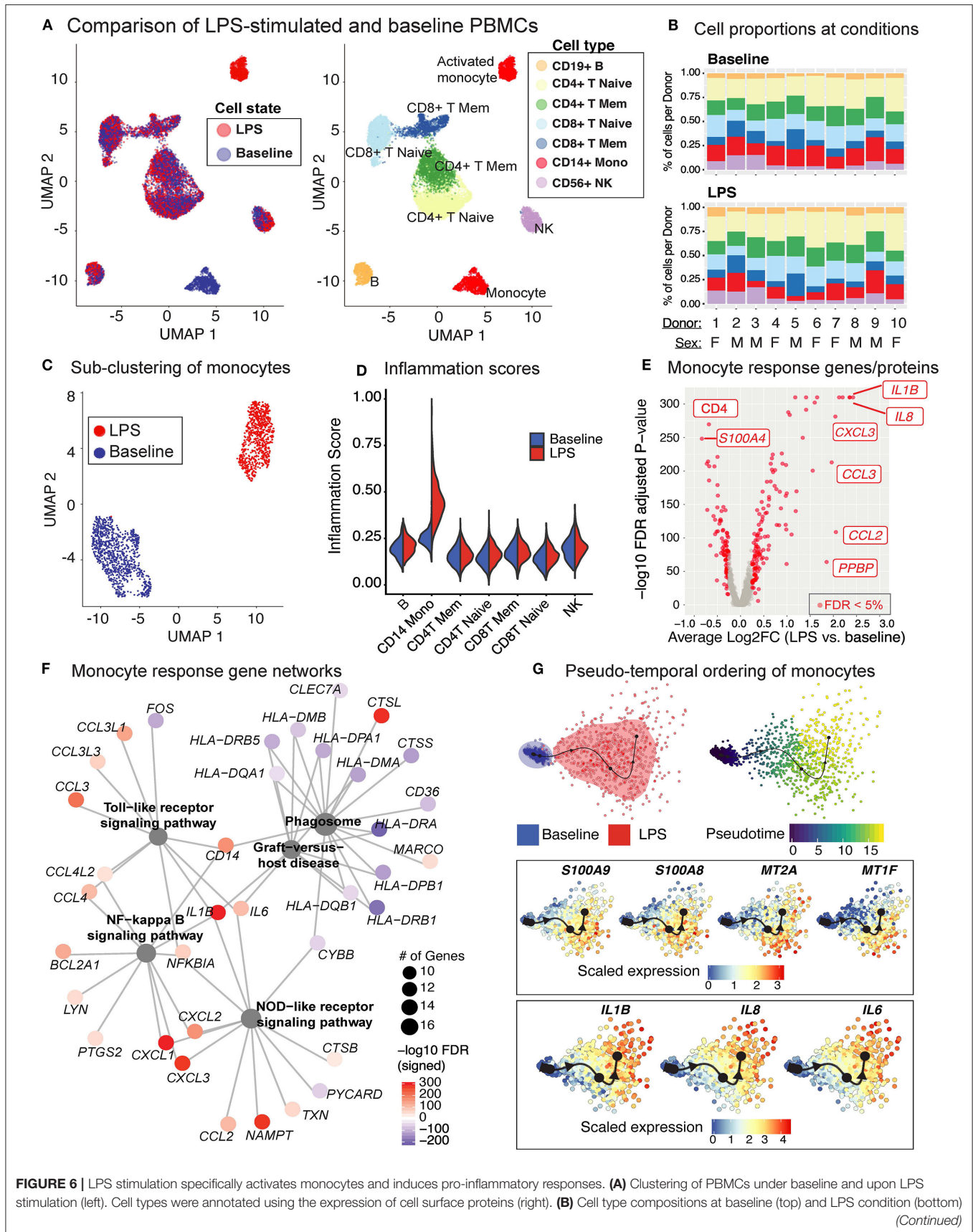


FIGURE 6 | across 10 donors. Refer to **(A)** for cell types' color coding. **(C)** Clustering of CD14⁺ monocytes separates baseline and LPS-stimulated cells. **(D)** Inflammation scores of all cells under two conditions. LPS-activated monocytes have the highest expression levels of inflammation-associated transcripts. **(E)** Differential expression analysis of LPS-stimulated and baseline monocytes revealed 125 induced and 94 reduced genes, respectively (FDR 5%), as well as 3 induced and 3 reduced proteins, respectively. **(F)** Enriched KEGG pathways (FDR 5%) for LPS response genes. Node size for each pathway represents the number of genes in the pathway that were also induced in LPS-stimulated monocytes. Node color for genes indicate induction (red) or reduction (blue) upon LPS treatment. LPS-activated monocytes upregulate genes associated with pattern recognition receptor signaling pathways (Toll-like receptor, NOD-like receptor) and inflammation (NF- κ B signaling), but also downregulate genes associated with antigen presentation and phagosome activity. **(G)** Trajectory (pseudotime) inference of monocytes under baseline and LPS conditions identified genes with heterogeneous activity in stimulated monocytes. Cells are color-coded with respect to activation status (top left) and inferred pseudotimes (top right). Expression levels of selected genes were overlaid on cells sorted in the activation trajectory (bottom).

and 47 genes uniquely induced in these states, respectively, compared to baseline (**Supplementary Figures 4C,D, Supplementary Table 7**).

Network analyses of genes induced in LPS2 and LPS3 states using Ingenuity Pathway Analysis (IPA; section Methods) revealed that LPS2 genes included alarmins (*S100A8*, *S100A9*) and genes associated with cell movement and trafficking (**Figure 7D**; genes in bold text, pink outline), such as various chemoattractants *CXCL7* (*PPBP*), *CCL7*, and *CCL8*. In contrast, LPS3 genes included pro-inflammatory interleukins (e.g., *IL1A*, *IL1B*, *IL6*), macrophage inflammatory protein-1-alpha (*CCL3*), -1-beta (*CCL4*), and -3 (*CCL20*), and tumor necrosis-associated factors (*TNFAIP6*, *TNIP1*) (**Figure 7E**). Interestingly, in LPS3, we also observed the induction of anti-inflammatory genes including *IL10*, *HLA-E*—an MHC class I molecule with inhibitory effects on cytokine production in monocytes (46), *IDO1*—an immunosuppressive enzyme - and one of its regulators *PTGS2* (47), suggesting a feedback loop to control increased inflammation. Pathway enrichment analysis using IPA disease and function terms verified that pro-inflammatory signals emerge at LPS2 state and peak at the later LPS3 state (**Supplementary Figure 4E**). At baseline, monocytes showed higher relative expression of ribosomal protein genes (**Supplementary Figure 4F**) and genes involved in mRNA processing, translation, and protein synthesis. Thus, scRNAseq analysis further delineates how LPS activates monocytes into early and late inflammatory states.

DISCUSSION

In vitro activation of circulating immune cells have been widely used for immune monitoring and identification of disease mechanisms since 1980s (8, 48). However, such assays are generally limited in scope and often only provide information regarding a single cell type. A holistic study of circulating immune cell responses to activators will uncover how the system as a whole respond to an immune challenge and how cell-cell interactions contribute to these responses. Hence these studies will bring us closer to a better understanding of immune cell responses in health and disease. CITE-seq enables precise studies of *in vivo* and *in vitro* immune cell responses. However, these assays are costly to generate and harbor technical challenges that might confound data interpretation (i.e., multiplets, batch effects). Herein we describe a cost-effective and in-depth study to uncover responses of peripheral blood mononuclear cells (PBMCs) from 10 healthy donors (5 men, 5 women) to two

widely used activators—anti-CD3/CD28 and LPS—to activate adaptive and innate cells, respectively. PBMCs were profiled using CITE-seq technology with 39 antibodies before and after activation; libraries were multiplexed using both cell hashing and genotypes, which permitted the super-loading of cells to reduce costs and batch effects (49). This design enabled studying activated cells in a cost-effective manner while also detecting and labeling multiplets from (i) different conditions, (ii) different individuals; and (iii) different cell types. We observed an increase in biological multiplets upon activation, potentially due to increased cell-cell interactions, which should be taken into consideration in future study designs to decouple biological (i.e., cellular interactions) from technical (i.e., due to super-loading) multiplets (50, 51). One caveat of multiplexing many libraries is the limited number of cells detected per donor (~1,600 cells), which was enough to study responses of major cell populations (e.g., CD14⁺ monocytes), but not that of less abundant ones (e.g., CD16⁺ monocytes, dendritic cells). Multiplexing fewer samples can effectively address this caveat in future studies.

Anti-CD3/CD28 treatment activated all classes of lymphocytes either directly (T cells) or indirectly (B, NK cells). Upon activation, co-stimulatory molecules (CD28, CD278) and activation markers (CD69, CD25) were expressed on the surface of both naïve and memory T cells. Transcriptomic changes in naïve T cells were the greatest likely due the fact that these cells start from a “lower transcriptional state” compared to their memory counterparts as they need to differentiate and initiate clonal expansion (52). Activated T cells highly expressed senescence (e.g., *CDKN1A*—encoding p21, *CDKN2A*—encoding p16, *SESN2*, and *PRKAA1*), effector and cytotoxic molecules (e.g., *GZMA/B/H*, *IFNG*). Using CITE-seq antibodies, under baseline conditions, we detected distinct subsets of memory cells (e.g., Th subsets, MAIT). However, these subsets were not detected upon activation, potentially due to the internalization of cell surface molecules and increased transcriptional similarity between memory subsets.

Indirect activation of NK cells *via* anti-CD3/CD28 activated 74 genes, most of which were shared with T cell responses including CD69, interferon stimulated/response, and cytotoxic genes. Scoring of single cells using different gene sets showed that activated NK cells had the highest scores for cytotoxicity whereas activated T cells had highest scores for senescence. Clustering and trajectory analyses revealed heterogeneity among activated NK and B cells. Late stage activated NK cells resembled previously described “helper” NK cells and expressed CD83 protein (35), whereas late stage activated B cells expressed molecules that

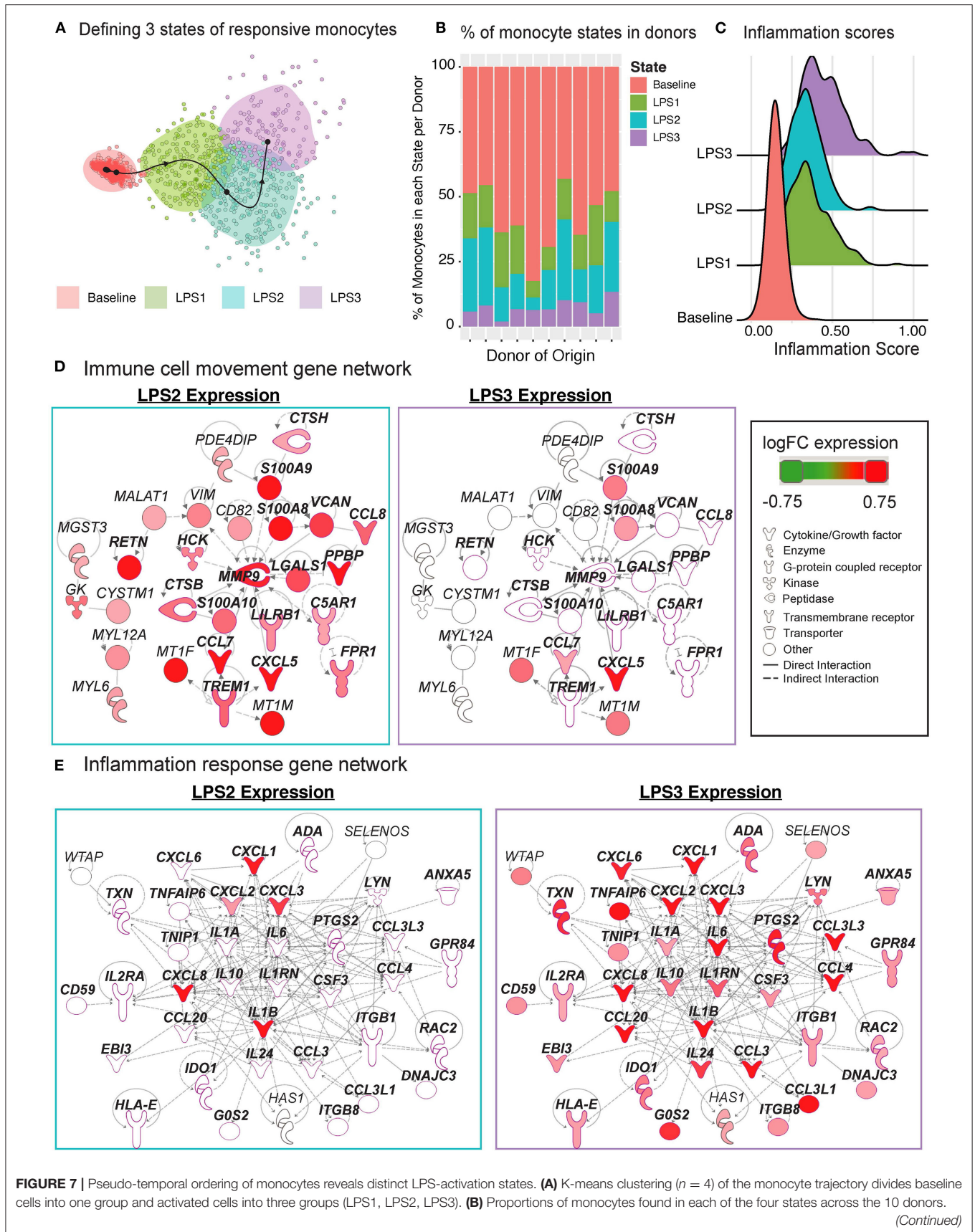


FIGURE 7 | Pseudo-temporal ordering of monocytes reveals distinct LPS-activation states. **(A)** K-means clustering ($n = 4$) of the monocyte trajectory divides baseline cells into one group and activated cells into three groups (LPS1, LPS2, LPS3). **(B)** Proportions of monocytes found in each of the four states across the 10 donors. *(Continued)*

FIGURE 7 | (C) Inflammation scores of monocytes in distinct states. LPS3 state monocytes show the highest average inflammation score. **(D)** Network of genes induced in activated monocytes from LPS2 state using Ingenuity Pathway Analysis (IPA). Molecules in bold are associated with immune cell migration and chemotaxis. **(E)** Network of genes induced in LPS3 activated monocytes. Bolded molecules are associated with inflammatory responses. For both networks, molecules with different functions were depicted with different shapes, as provided by IPA. Molecules are colored based on their log₂ fold change in expression in that state vs. all other baseline and activated states. Direct and indirect gene interactions are depicted by solid and dashed lines, respectively.

have been expressed in B cells associated with aging and auto-immune diseases (*TLR7*, *PRDM1*, *ITGAX/CD11c*, *TBX21/T-bet*) (39–41). However, compared to DN2s and ABCs, activated B cells retained follicular and conventional memory markers (*CXCR5* and *CD27*), likely as a reflection of acute vs. chronic activation. Future single cell activation studies from different populations should help further characterize these B cells.

LPS stimulation specifically activated monocytes and pseudo-temporal analyses uncovered two states of activated monocytes: (i) a first state that includes pro-inflammatory alarmins (*S100A8/A9*) and molecules to attract and interact with other immune cells (*PPBP*, *CCL7*, *CCL8*); and (ii) a second, possibly more terminated inflammatory state, with increased expression of *bona fide* inflammatory cytokines (*IL1B*, *IL6*, *IL8*, and *IL24*) and potential anti-inflammatory molecules (*IL-10*, *SOCS3*, *HLA-E*, and *IDO1*) to mitigate the effects of increased inflammation. A similar phenomenon was noted in human blood dendritic cell subsets in which cellular responses to influenza virus infection resulted in three waves of chemokine secretion to attract effector immune cells (53). Induction of interferon response genes and TFs (*STAT1* and *IRF1*) previously reported in IFN-g-primed (24 h) (54) and LPS-induced (0–4 h) monocytes (43), was not observed in our study, potentially due to the 24-h stimulation, which is a later time-point in the activation cascade. Anti-CD3/CD28 treatment reduced the numbers of monocytes in PBMCs likely due to the induced apoptosis *via* activated T cells (28). LPS treatment had no effect on B cells because B cells from healthy human donors lack TLR4 on their surfaces (55–59) and respond poorly to TLR4 (60, 61).

In summary, this study provides an experimental and computational framework to carefully study activated immune cells using single cell methods by multiplexing to handle batch effects and cut costs and by quantifying protein expression to identify cell types, cell states, and multiplet cells. The data, analyses, and application developed here will be important resources for future studies such as exposure of immune cells to antigens, microbes, adjuvants and other targeting agents. It will guide the design of subsequent experiments to further expand our understanding of cellular responses to additional *in vivo* and *in vitro* activation conditions in healthy and diseased individuals. Overall, this study provides a foundation for future immune activation experiments using single cell technologies. The data is freely shared via Human Cell Atlas platform as well as via an interactive R shiny application (<https://czi-pbmc-cite-seq.jax.org/>).

METHODS

Blood Collection

Blood was collected at the UConn Health Clinical Research Center (CRC) at 263 Farmington Avenue Farmington, CT

06030-3805 following informed consent of participants for a UConn Health IRB-approved protocol (IRB Number: 18-151J-2). Approximately 50 ml of blood was collected from each donor. Samples were collected BD vacutainer tubes containing Acid Citric Dextrose (ACD) Solution A, and peripheral blood mononuclear cells (PBMC) were isolated immediately after.

Isolation and Stimulation of PBMCs

Peripheral blood mononuclear cells (PBMCs) were isolated with gradient centrifugation using Lymphoprep (StemCell Technologies) and the red blood cells were removed by incubating the cells with RBC lysis buffer (Tonbo Biosciences). After that, the PBMCs were immediately cultured using activation conditions described below for 24 h at 1 million cells/ml density in complete RPMI (RPMI supplemented with 10% heat-inactivated Fetal bovine serum, 100 U/ml Penicillin/Streptomycin, 2 mM L-glutamine, 10 mM HEPES, 0.1 mM Non-essential amino acids, 1 mM Sodium pyruvate) at 37°C + 5% CO₂. The PBMCs were cultured in three different ways: (1) Plate-bound anti-CD3 + anti-CD28 (clones OKT3 and CD28.2 at 2 μg/ml each—Tonbo Biosciences)—plates were coated with Goat anti-mouse IgG (clone Poly4053 at 10 μg/ml—BioLegend) for 1 h at 37°C, washed, then coated with both anti-CD3 and anti-CD28 also for 1 h at 37°C. After that cells were added to the plates for stimulation; (2) lipopolysaccharide (LPS) (10 ng/ml—InvivoGen); and (3) Complete medium only as control. After 24 h in culture, an aliquot of each sample was stained for flow cytometry analysis and the remaining cells were harvested and frozen for subsequent CITE-seq analysis and genotyping.

Flow Cytometry and Antibodies

PBMCs cells were incubated with Ghost Dye™ Violet 510 (Tonbo Biosciences) to stain dead cells for 10 min at room temperature (RT). After, Fc receptors were blocked for 5 min at RT using FcR-blocking reagent (Miltenyi Biotec) and then incubated with fluorochrome-conjugated surface antibodies for 15 min at RT. The surface antibodies CD3 (UCHT1), CD11b (M1/70), CD14 (HCD14), CD16 (3G8), CD19 (HIB19), CD20 (2H7), CD25 (BC96), CD27 (O323), CD69 (FN50), HLA-DR/MHC class II (L243) were all from BioLegend and CD80 (2D10.4) from eBioscience. FACS analysis was performed on a BD LSR Fortessa (BD Biosciences) and data were analyzed with FlowJo software (Version 10.2, TreeStar).

CITE-seq Data Generation With Cell Hashing

CITE-seq data was generated from 30 samples (10 individuals, 3 experimental conditions) by multiplexing to reduce batch effects and costs using cell hashing (49) (for experimental conditions)

and genotype-based demultiplexing (27) (for individual donors). For CITE-seq experiments, antibody-oligo conjugates against 39 surface proteins (e.g., CD8, CD45RA, CD4, CD3, CCR7, CD69) as well as the Cell Hashing Antibodies (HTOs) were purchased from BioLegend. PBMCs from different donors were independently stained with one of our HTO-conjugated antibody pools (based on the experimental condition) and a pool of 39 immunophenotypic markers for CITE-seq. Equal numbers of cells from all 30 samples were pooled and super-loaded onto 10 lanes of 10× Genomics Single Cell 3P v2 (10× Genomics, USA), yielding approximately 25 K cells per lane. All libraries were sequenced together on Illumina NovaSeq S4 flowcells.

Genotyping of PBMCs

PBMCs from 10 donors were genotyped using Infinium Omni2.5-8 v1.3 BeadChip Array (Illumina) according to manufacturer's instructions. We mapped the Illumina array probe sequences to hg19 genome assembly and excluded potential problematic ones as in (62, 63). Furthermore, we filtered out SNPs with an alternate allele frequency difference with 1000G EUR samples > 20%, or palindromic SNPs with a minor allele frequency > 20%, genotype missingness > 2.5%, Hardy-Weinberg $p < 10^{-4}$. Finally, 1,147,545 genotyped SNPs were considered for further analyses.

Sample Demultiplexing Using Cell Hashing

Three hashtag oligonucleotides (HTO) were used to multiplex samples from different experimental conditions (e.g., HTO A for baseline samples; HTO B for Anti-CD3/CD28 treated samples). Cell HTOs were counted in raw sequencing data using CITE-seq-Count version 1.4.2. (49). CITE-seq-Count was used to count HTOs for each cell using recommended parameter settings (“-cells 25,000 -cbf 1 -cbl 16 -umif 17 -umil 26 -max-error 3”). HTO counts per cell were normalized with respect to the total read counts for that cell and scaled and log2 transformed. Distributions of read counts for each HTO across all cells were bimodal. To classify whether a cell has detectable counts for an HTO, we fit a Gaussian mixture model (with 2 mixture components) for each HTO using mclust R package (64) (version 5.4.5). Based on these models, we labeled each cell as: (i) empty: if there are no sufficient read counts for any HTO; (ii) singlet: only if counts for a single HTO were detected; (iii) multiplets: if there are detectable counts for 2 (“doublet”) or 3 (“triplet”).

Sample Demultiplexing With Demuxlet

Genotypes were used to demultiplex the donor of origin for each sample using Demuxlet version 2 (27) with default parameters. For this we used 167,703 genotyped SNPs overlapping exonic regions in the genome. Cells annotated to one individual were retained, while “ambiguous” and “doublet” cells were discarded from further analyses.

RNA Quantification

Single cell RNA-sequencing libraries were prepared using the Chromium Single Cell 3' Reagent Kit (v2 Chemistry) according

to the user guide (10× Genomics). Resulting libraries were sequenced using Illumina NovaSeq S4 flowcells to an average depth of ~150,000 reads per cell. Reads were aligned to human reference sequence GRCh37/hg19 and unique molecular identifiers (UMIs) were quantified using the Cell Ranger “count” software (10× Genomics, version 2.1.0) and with additional parameters “-expect-cells=25000.” Cell barcodes with fewer than 400 detected genes, and those not identified to be singlets via cell hashing or Demuxlet were discarded from analyses.

Protein Quantification

Read counts for antibody derived tags (ADTs) for 39 distinct antibodies were measured from raw sequencing reads using CITE-seq-Count with the following parameters: “-cells 25,000 -cbf 1 -cbl 16 -umif 17 -umil 26 -max-error 3”. Raw counts were normalized using a centered log ratio approach using Seurat R package version 3.0.2 (65).

Multiplet Cell Removal Using Surface Protein Expression

Number of multiplet cells increases upon activation, due to the increase in cell-cell interactions. To remove such multiplets, we took advantage of cell surface protein expression levels and identified cells that co-expressed multiple cell-type-specific proteins. First, we determined which cells were “positive” and “negative” for each protein using the HTODemux function from Seurat (65). Since some immune cells co-express certain cell surface markers (e.g., NK and CD8⁺ T cells both express CD8), we devised a multiplet removal protocol for each cell type. For B cell multiplets, we filtered out cells that express CD19 in addition to one of the following (i) a T cell marker (CD3, CD4, CD8); (ii) an innate cell marker (CD14, CD16, CD56). For CD14⁺ monocyte multiplets, we removed cells that express CD14 and (i) a T cell marker (CD3, CD8, CD28); (ii) NK marker CD56; (iii) a B cell marker (CD19, CD20). For NK cell multiplets, we removed cells that are positive for CD56 and one or more of the following (i) T cell markers (CD3, CD4, CD28); (ii) monocyte markers (CD14, CD11c); (iii) B cell markers (CD19, CD20). For CD4⁺ T cell multiplets, we removed cells that express CD4 markers (CD3, CD4) and one or more of the following (i) CD8 (for CD8⁺ T), CD56 (for NK), CD19, CD20 (for B cells), CD14, CD16 (for monocytes/NK). Lastly, for CD8⁺ T cell multiplets, we removed cells that co-expressed CD8 markers (CD3, CD8) and one or more of the following (i) CD4 (for CD4⁺ T cells), (ii) CD56 (for NK), (iii) CD19, CD20 (for B cells), and (iv) CD14, CD16 (for monocytes/NK). After all cells are removed we obtained comparable number of single cells for each individual upon 3 conditions. These cell numbers correlated significantly with cell numbers inferred from flow cytometry data ($R = 0.97$).

Cell Clustering

Cells were clustered using top 500 most variable genes and proteins, which are determined by fitting a line to the relationship of the variance and mean using a local polynomial regression (loess). Protein/gene expression values were standardized using

the observed normalized mean and expected variance (given by the fitted line). Feature variance was then calculated on the standardized values after clipping to a maximum of the square root of the number of cells. After scaling and centering the feature values, principal component analysis (PCA) was performed on the top 500 variable features. Following this, uniform manifold approximation and projection (UMAP) was applied on the top 20 principal components to reduce the data to two dimensions. Next, a shared nearest neighbor (SNN) graph was created by calculating the neighborhood (Jaccard index) overlap between each cell and its 20 (default) nearest neighbors. To identify cell clusters, we used a SNN modularity optimization based clustering algorithm (66).

Differential Expression

To identify cell-type-specific response genes and proteins, we conducted pairwise Wilcoxon Rank Sum tests between each PBMC cell-type under stimulation and baseline conditions (e.g., LPS stimulated monocytes vs. baseline monocytes). In each differential expression analysis, genes detected in at least 10% of each cell group were considered. Features with an absolute difference in expression $> \log_2(0.25)$ and false discovery rate $< 5\%$ were regarded as significant results.

Single Cell Pseudo-Temporal Trajectory Inference

Benchmarking and inference of single cell pseudotime trajectories were performed with the R package *dyno* (version 0.1.1) (67). Briefly, for each cell-specific response (e.g., monocytes induced by LPS) trajectories were inferred using Slingshot (the method determined to minimize error and maximize scalability and accuracy). Pseudo-temporal ordering of cells were derived using the corresponding baseline and activated cells as well as the genes and ADTs previously determined to be differentially induced (FDR $< 5\%$) between the two groups of cells.

Ingenuity Pathway Analysis

Response genes were uploaded to Qiagen's Ingenuity Pathway Analysis (IPA) version 01-16 system to build gene networks for each gene set. Networks were constructed using the Connect tool with "Human" as the species parameter and otherwise default parameters to map direct and indirect interactions between molecules as described in the Ingenuity Knowledge Base (IKB). IPA's core analysis function was also used to annotate each response gene set and resultant networks with canonical pathways, relevant diseases, and biological functions.

Single Cell Scoring

Genes associated with inflammation were obtained from NanoString Technologies, Inc. (cite, <https://www.nanostring.com/products/gene-expression-panels/gene-expression-panels-overview/ncounter-inflammation-panels>) and used to calculate

an inflammation score for PBMCs at baseline and LPS-stimulated conditions. Feature counts for each cell were divided by the total counts for that cell, multiplied by a scale factor of 10,000, and then log normalized. Normalized read counts for all inflammation-associated genes were divided by the normalized counts of all transcripts and then min-max scaled between 0 and 1. Gene lists (**Supplementary Table 3**) were used to score cytotoxicity, MAIT or senescence expressions across T and NK cell clusters. To do so, we calculated the mean expression for each cell, within each cluster.

Pathway Analysis of Stimulation-Response Genes

Differentially expressed genes for each cell-type-response to stimulation were functionally annotated using the R package *clusterProfiler* (version 3.14.0) (42). The Kyoto Encyclopedia of Genes and Genomes (KEGG), gene ontology (GO), and WikiPathways databases were used to determine association with particular biological processes, diseases, and molecular functions. The top pathways with an FDR-adjusted $p < 5\%$ were summarized in the results.

DATA AVAILABILITY STATEMENT

The datasets presented in this study can be found in online repositories. The names of the repository/repository and accession number(s) can be found at: <https://www.ebi.ac.uk/ena>, PRJEB40448; <https://www.ebi.ac.uk/ena>, ERZ1631464; <https://www.ebi.ac.uk/ena>, PRJEB40376.

ETHICS STATEMENT

The studies involving human participants were reviewed and approved by UConn Health IRB-approved protocol (IRB Number: 18-151J-2). The patients/participants provided their written informed consent to participate in this study.

AUTHOR CONTRIBUTIONS

DU, AW, MS, and PS designed the experimental study design. MS, PS, AW, and JG processed PBMC samples and the sequencing of libraries. NL and DN-B performed bioinformatics analyses of the data. NL, DU, AW, DN-B, MLS, VP, and JB interpreted the data. NL, JB, AW, and DU wrote the manuscript. NL, JB, DN-B, AW, and DU designed the corresponding figures. NL created the R shiny web application. All authors edited and reviewed the manuscript prior to submission.

FUNDING

This work was funded by a grant from Chan-Zuckerberg Initiative and Silicon Valley Community Foundation [2018-182753 (5022) to DU] and Jackson Laboratory funds to DU,

AW, NL, JB, and DN-B were partly supported by RO-1 NIA and NIAID.

ACKNOWLEDGMENTS

We thank all members of the Stitzel and Ucar labs for constructive feedback and discussion on this study and manuscript. We also thank members of the Human Cell Atlas

data wrangler team for assistance with depositing the data associated with this manuscript.

SUPPLEMENTARY MATERIAL

The Supplementary Material for this article can be found online at: <https://www.frontiersin.org/articles/10.3389/fimmu.2021.636720/full#supplementary-material>

REFERENCES

- Sen P, Kemppainen E, Orešič M. Perspectives on systems modeling of human peripheral blood mononuclear cells. *Front Mol Biosci.* (2018) 4:96. doi: 10.3389/fmolb.2017.00096
- Schmiedel BJ, Singh D, Madrigal A, Valdovino-Gonzalez AG, White BM, Zapardiel-Gonzalo J, et al. Impact of genetic polymorphisms on human immune cell gene expression. *Cell.* (2018) 175:1701–15.e16. doi: 10.1016/j.cell.2018.10.022
- Kotliarov Y, Sparks R, Martins AJ, Mulè MP, Lu Y, Goswami M, et al. Broad immune activation underlies shared set point signatures for vaccine responsiveness in healthy individuals and disease activity in patients with lupus. *Nat Med.* (2020) 26:618–29. doi: 10.1038/s41591-020-0769-8
- Moskowitz DM, Zhang DW, Hu B, Le Saux S, Yanes RE, Ye Z, et al. Epigenomics of human CD8 T cell differentiation and aging. *Sci Immunol.* (2017) 2:eaag0192. doi: 10.1126/sciimmunol.aag0192
- Banchereau R, Hong S, Cantarel B, Baldwin N, Baisch J, Edens M, et al. Personalized immunomonitoring uncovers molecular networks that stratify lupus patients. *Cell.* (2016) 165:551–65. doi: 10.1016/j.cell.2016.03.008
- Persson U, Johansson SG. Concanavalin A-induced activation of human T cell subpopulations. *Int Arch Allergy Appl Immunol.* (1984) 75:337–44. doi: 10.1159/000233644
- Trickett A, Kwan YL. T cell stimulation and expansion using anti-CD3/CD28 beads. *J Immunol Methods.* (2003) 275:251–5. doi: 10.1016/S0022-1759(03)00010-3
- Smith-Garvin JE, Koretzky GA, Jordan MS. T cell activation. *Annu Rev Immunol.* (2009) 27:591–619. doi: 10.1146/annurev.immunol.021908.132706
- Rossol M, Heine H, Meusch U, Quandt D, Klein C, et al. LPS-induced cytokine production in human monocytes and macrophages. *Crit Rev Immunol.* (2011) 31:379–446. doi: 10.1615/critrevimmunol.v31.i5.20
- Cepika A-M, Banchereau R, Segura E, Ohouo M, Cantarel B, Goller K, et al. A multidimensional blood stimulation assay reveals immune alterations underlying systemic juvenile idiopathic arthritis. *J Exp Med.* (2017) 214:3449–66. doi: 10.1084/jem.20170412
- Piasecka B, Duffy D, Urrutia A, Quach H, Patin E, Posseme C, et al. Distinctive roles of age, sex, and genetics in shaping transcriptional variation of human immune responses to microbial challenges. *Proc Natl Acad Sci USA.* (2018) 115:E488–97. doi: 10.1073/pnas.1714765115
- Thomas S, Rouilly V, Patin E, Alanio C, Dubois A, Delval C, et al. The Milieu Intérieur study - an integrative approach for study of human immunological variance. *Clin Immunol.* (2015) 157:277–93. doi: 10.1016/j.clim.2014.12.004
- Molony RD, Nguyen JT, Kong Y, Montgomery RR, Shaw AC, Iwasaki A. Aging impairs both primary and secondary RIG-I signaling for interferon induction in human monocytes. *Sci Signal.* (2017) 10:eaan2392. doi: 10.1126/scisignal.aan2392
- Shaw AC, Goldstein DR, Montgomery RR. Age-dependent dysregulation of innate immunity. *Nat Rev Immunol.* (2013) 13:875–87. doi: 10.1038/nri3547
- Shaw AC, Panda A, Joshi SR, Qian F, Allore HG, Montgomery RR. Dysregulation of human Toll-like receptor function in aging. *Ageing Res Rev.* (2011) 10:346–53. doi: 10.1016/j.arr.2010.10.007
- Qian F, Guo X, Wang X, Yuan X, Chen S, Malawista SE, et al. Reduced bioenergetics and Toll-like receptor 1 function in human polymorphonuclear leukocytes in aging. *Ageing (Albany NY).* (2014) 6:131–9. doi: 10.18632/aging.100642
- Gowthaman U, Chen JS, Zhang B, Flynn WF, Lu Y, Song W, et al. Identification of a T follicular helper cell subset that drives anaphylactic IgE. *Science.* (2019) 365:eaaw6433. doi: 10.1126/science.aaw6433
- Papalexi E, Satija R. Single-cell RNA sequencing to explore immune cell heterogeneity. *Nat Rev Immunol.* (2018) 18:35–45. doi: 10.1038/nri.2017.76
- Regev A, Teichmann SA, Lander ES, Amit I, Benoist C, Birney E, et al. The human cell atlas. *Elife.* (2017) 6:e27041. doi: 10.7554/eLife.27041
- Pereira BI, De Maeyer RPH, Covre LP, Nehar-Belaid D, Lanna A, Ward S, et al. Sestrins induce natural killer function in senescent-like CD8⁺ T cells. *Nat Immunol.* (2020) 21:684–94. doi: 10.1038/s41590-020-0643-3
- Szabo PA, Levitin HM, Miron M, Snyder ME, Senda T, Yuan J, et al. Single-cell transcriptomics of human T cells reveals tissue and activation signatures in health and disease. *Nat Commun.* (2019) 10:4706. doi: 10.1038/s41467-019-12464-3
- Shalek AK, Satija R, Shuga J, Trombetta JJ, Gennert D, Lu D, et al. Single-cell RNA-seq reveals dynamic paracrine control of cellular variation. *Nature.* (2014) 510:363–9. doi: 10.1038/nature13437
- Villani A-C, Satija R, Reynolds G, Sarkizova S, Shekhar K, Fletcher J, et al. Single-cell RNA-seq reveals new types of human blood dendritic cells, monocytes, and progenitors. *Science.* (2017) 356:eaah4573. doi: 10.1126/science.aah4573
- Horns F, Dekker CL, Quake SR. Memory B cell activation, broad anti-influenza antibodies, and bystander activation revealed by single-cell transcriptomics. *Cell Rep.* (2020) 30:905–13.e6. doi: 10.1016/j.celrep.2019.12.063
- Nehar-Belaid D, Hong S, Marches R, Chen G, Bolisetty M, Baisch J, et al. Mapping systemic lupus erythematosus heterogeneity at the single-cell level. *Nat Immunol.* (2020) 21:1094–106. doi: 10.1038/s41590-020-0743-0
- Stoeckius M, Hafemeister C, Stephenson W, Houck-Loomis B, Chattopadhyay PK, Swerdlow H, et al. Simultaneous epitope and transcriptome measurement in single cells. *Nat Methods.* (2017) 14:865–8. doi: 10.1038/nmeth.4380
- Kang HM, Subramaniam M, Targ S, Nguyen M, Maliskova L, McCarthy E, et al. Multiplexed droplet single-cell RNA-sequencing using natural genetic variation. *Nat Biotechnol.* (2018) 36:89–94. doi: 10.1038/nbt.4042
- Jagger AL, Evans HG, Walter GJ, Gullick NJ, Menon B, Ballantine LE, et al. FAS/FAS-L dependent killing of activated human monocytes and macrophages by CD4⁺CD25⁻ responder T cells, but not CD4⁺CD25⁺ regulatory T cells. *J Autoimmun.* (2012) 38:29–38. doi: 10.1016/j.jaut.2011.11.015
- Kaplan MJ, Ray D, Mo RR, Yung RL, Richardson BC. TRAIL (Apo2 ligand) and TWEAK (Apo3 ligand) mediate CD4⁺ T cell killing of antigen-presenting macrophages. *J Immunol.* (2000) 164:2897–904. doi: 10.4049/jimmunol.164.6.2897
- Morita R, Schmitt N, Bentebibel S-E, Ranganathan R, Bourdery L, Zurawski G, et al. Human blood CXCR5⁺CD4⁺ T cells are counterparts of t follicular cells and contain specific subsets that differentially support antibody secretion. *Immunity.* (2011) 34:108–21. doi: 10.1016/j.immuni.2010.12.012
- Kim CH, Rott L, Kunkel EJ, Genovese MC, Andrew DP, Wu L, et al. Rules of chemokine receptor association with T cell polarization *in vivo*. *J Clin Invest.* (2001) 108:1331–9. doi: 10.1172/JCI13543
- Tian Y, Babor M, Lane J, Schulten V, Patil VS, Seumois G, et al. Unique phenotypes and clonal expansions of human CD4 effector memory T cells re-expressing CD45RA. *Nat Commun.* (2017) 8:1473. doi: 10.1038/s41467-017-01728-5

33. Park D, Kim HG, Kim M, Park T, Ha H-H, Lee DH, et al. Differences in the molecular signatures of mucosal-associated invariant T cells and conventional T cells. *Sci Rep.* (2019) 9:7094. doi: 10.1038/s41598-019-43578-9
34. Street K, Rizzo D, Fletcher RB, Das D, Ngai J, Yosef N, et al. Slingshot: cell lineage and pseudotime inference for single-cell transcriptomics. *BMC Genomics.* (2018) 19:477. doi: 10.1186/s12864-018-4772-0
35. Mailliard RB, Alber SM, Shen H, Watkins SC, Kirkwood JM, Herberman RB, et al. IL-18-induced CD83⁺CCR7⁺ NK helper cells. *J Exp Med.* (2005) 202:941–53. doi: 10.1084/jem.20050128
36. Robertson MJ. Role of chemokines in the biology of natural killer cells. *J Leukoc Biol.* (2002) 71:173–83.
37. Rabacal W, Pabbisetty SK, Hoek KL, Cendron D, Guo Y, Maseda D, et al. Transcription factor KLF2 regulates homeostatic NK cell proliferation and survival. *Proc Natl Acad Sci USA.* (2016) 113:5370–5. doi: 10.1073/pnas.1521491113
38. Hao Y, O'Neill P, Naradikian MS, Scholz JL, Cancro MP. A B-cell subset uniquely responsive to innate stimuli accumulates in aged mice. *Blood.* (2011) 118:1294–304. doi: 10.1182/blood-2011-01-330530
39. Rubtsova K, Rubtsov AV, Thurman JM, Mennona JM, Kappler JW, Marrack P. B cells expressing the transcription factor T-bet drive lupus-like autoimmunity. *J Clin Invest.* (2017) 127:1392–404. doi: 10.1172/JCI91250
40. Zhang W, Zhang H, Liu S, Xia F, Kang Z, Zhang Y, et al. Excessive CD11c⁺Tbet⁺ B cells promote aberrant TFH differentiation and affinity-based germinal center selection in lupus. *Proc Natl Acad Sci USA.* (2019) 116:18550–60. doi: 10.1073/pnas.1901340116
41. Jenks SA, Cashman KS, Zumaquero E, Marigorta UM, Patel AV, Wang X, et al. Distinct effector B cells induced by unregulated Toll-like receptor 7 contribute to pathogenic responses in systemic lupus erythematosus. *Immunity.* (2018) 49:725–39.e6. doi: 10.1016/j.immuni.2018.08.015
42. Yu G, Wang L-G, Han Y, He Q-Y. clusterProfiler: an R Package for Comparing Biological Themes Among Gene Clusters. *OMICS.* (2012) 16:284–7. doi: 10.1089/omi.2011.0118
43. Baillie JK, Arner E, Daub C, De Hoon M, Itoh M, Kawaji H, et al. Analysis of the human monocyte-derived macrophage transcriptome and response to lipopolysaccharide provides new insights into genetic aetiology of inflammatory bowel disease. *PLoS Genet.* (2017) 13:e1006641. doi: 10.1371/journal.pgen.1006641
44. Schinnerling K, García-González P, Aguillón JC. Gene Expression profiling of human monocyte-derived dendritic cells—searching for molecular regulators of tolerogenicity. *Front Immunol.* (2015) 6:528. doi: 10.3389/fimmu.2015.00528
45. Crowe LAN, McLean M, Kitson SM, Melchor EG, Patommel K, Cao HM, et al. S100A8 & S100A9: alarmin mediated inflammation in tendinopathy. *Sci Rep.* (2019) 9:1463. doi: 10.1038/s41598-018-37684-3
46. Maeda A, Kawamura T, Ueno T, Usui N, Eguchi H, Miyagawa S. The suppression of inflammatory macrophage-mediated cytotoxicity and proinflammatory cytokine production by transgenic expression of HLA-E. *Transpl Immunol.* (2013) 29:76–81. doi: 10.1016/j.trim.2013.08.001
47. Hennequart M, Pilote L, Cane S, Hoffmann D, Stroobant V, Plaen ED, et al. Constitutive IDO1 expression in human tumors is driven by cyclooxygenase-2 and mediates intrinsic immune resistance. *Cancer Immunol Res.* (2017) 5:695–709. doi: 10.1158/2326-6066.CIR-16-0400
48. Hamilton RG, Adkinson NF. *In vitro* assays for the diagnosis of IgE-mediated disorders. *J Allergy Clin Immunol.* (2004) 114:213–25. doi: 10.1016/j.jaci.2004.06.046
49. Stoeckius M, Zheng S, Houck-Loomis B, Hao S, Yeung BZ, Mauck WM, et al. Cell Hashing with barcoded antibodies enables multiplexing and doublet detection for single cell genomics. *Genome Biol.* (2018) 19:224. doi: 10.1186/s13059-018-1603-1
50. Bendall SC. Diamonds in the doublets. *Nat Biotechnol.* (2020) 38:559–61. doi: 10.1038/s41587-020-0511-6
51. Giladi A, Cohen M, Medaglia C, Baran Y, Li B, Zada M, et al. Dissecting cellular crosstalk by sequencing physically interacting cells. *Nat Biotechnol.* (2020) 38:629–37. doi: 10.1038/s41587-020-0442-2
52. Cho BK, Wang C, Sugawa S, Eisen HN, Chen J. Functional differences between memory and naive CD8 T cells. *Proc Natl Acad Sci USA.* (1999) 96:2976–81. doi: 10.1073/pnas.96.6.2976
53. Piqueras B, Connolly J, Freitas H, Palucka AK, Banchereau J. Upon viral exposure, myeloid and plasmacytoid dendritic cells produce 3 waves of distinct chemokines to recruit immune effectors. *Blood.* (2006) 107:2613–8. doi: 10.1182/blood-2005-07-2965
54. Qiao Y, Giannopoulou EG, Chan CH, Park S, Gong S, Chen J, et al. Synergistic activation of inflammatory cytokine genes by interferon- γ -induced chromatin remodeling and Toll-like receptor signaling. *Immunity.* (2013) 39:454–69. doi: 10.1016/j.immuni.2013.08.009
55. Bource E, Bosisio D, Golay J, Polentarutti N, Mantovani A. The Toll-like receptor repertoire of human B lymphocytes: inducible and selective expression of TLR9 and TLR10 in normal and transformed cells. *Blood.* (2003) 102:956–63. doi: 10.1182/blood-2002-11-3355
56. Hornung V, Rothenfusser S, Britsch S, Krug A, Jahrsdörfer B, Giese T, et al. Quantitative expression of Toll-like receptor 1–10 mRNA in cellular subsets of human peripheral blood mononuclear cells and sensitivity to CpG oligodeoxynucleotides. *J Immunol.* (2002) 168:4531–7. doi: 10.4049/jimmunol.168.9.4531
57. Muzio M, Bosisio D, Polentarutti N, D'amico G, Stoppacciaro A, Mancinelli R, et al. Differential expression and regulation of Toll-like receptors (TLR) in human leukocytes: selective expression of TLR3 in dendritic cells. *J Immunol.* (2000) 164:5998–6004. doi: 10.4049/jimmunol.164.11.5998
58. Shin H, Zhang Y, Jagannathan M, Hasturk H, Kantarci A, Liu H, et al. B cells from periodontal disease patients express surface Toll-like receptor 4. *J Leukoc Biol.* (2009) 85:648–55. doi: 10.1189/jlb.0708428
59. Zarembek KA, Godowski PJ. Tissue expression of human Toll-like receptors and differential regulation of Toll-like receptor mRNAs in leukocytes in response to microbes, their products, and cytokines. *J Immunol.* (2002) 168:554–61. doi: 10.4049/jimmunol.168.2.554
60. Jagannathan M, Hasturk H, Liang Y, Shin H, Hetzel JT, Kantarci A, et al. TLR cross-talk specifically regulates cytokine production by B cells from chronic inflammatory disease patients. *J Immunol.* (2009) 183:7461–70. doi: 10.4049/jimmunol.0901517
61. Jagannathan M, McDonnell M, Liang Y, Hasturk H, Hetzel J, Rubin D, et al. Toll-like receptors regulate B cell cytokine production in patients with diabetes. *Diabetologia.* (2010) 53:1461–71. doi: 10.1007/s00125-010-1730-z
62. Lawlor N, Márquez EJ, Orchard P, Narisu N, Shamim MS, Thibodeau A, et al. Multiomic profiling identifies cis-regulatory networks underlying human pancreatic β cell identity and function. *Cell Rep.* (2019) 26:788–801.e6. doi: 10.1016/j.celrep.2018.12.083
63. Varshney A, Scott LJ, Welch RP, Erdos MR, Chines PS, Narisu N, et al. Genetic regulatory signatures underlying islet gene expression and type 2 diabetes. *Proc Natl Acad Sci USA.* (2017) 114:2301–6. doi: 10.1073/pnas.1621192114
64. Scrucca L, Fop M, Murphy TB, Raftery AE. mclust 5: Clustering, Classification and Density Estimation Using Gaussian Finite Mixture Models. *R J.* (2016) 8:289–317. doi: 10.32614/rj-2016-021
65. Butler A, Hoffman P, Smibert P, Papalexis E, Satija R. Integrating single-cell transcriptomic data across different conditions, technologies, and species. *Nat Biotechnol.* (2018) 36:411–20. doi: 10.1038/nbt.4096
66. Blondel VD, Guillaume J-L, Lambiotte R, Lefebvre E. Fast unfolding of communities in large networks. *J Stat Mech.* (2008) 2008:P10008. doi: 10.1088/1742-5468/2008/10/P10008
67. Saelens W, Cannoodt R, Todorov H, Saeys Y. A comparison of single-cell trajectory inference methods. *Nat Biotechnol.* (2019) 37:547–54. doi: 10.1038/s41587-019-0071-9

Conflict of Interest: The authors declare that the research was conducted in the absence of any commercial or financial relationships that could be construed as a potential conflict of interest.

Copyright © 2021 Lawlor, Nehar-Belaid, Grassmann, Stoeckius, Smibert, Stitzel, Pascual, Banchereau, Williams and Ucar. This is an open-access article distributed under the terms of the Creative Commons Attribution License (CC BY). The use, distribution or reproduction in other forums is permitted, provided the original author(s) and the copyright owner(s) are credited and that the original publication in this journal is cited, in accordance with accepted academic practice. No use, distribution or reproduction is permitted which does not comply with these terms.